ELSEVIER

Journal of Nuclear Materials 313–316 (2003) 980–985

journal of nuclear materials

www.elsevier.com/locate/jnucmat

Divertor detachment during pure helium plasmas in JET

M. Wischmeier [a,*], D. Coster [b], X. Bonnin [c], T. Eich [b], A. Huber [d], C. Ingesson [e], S. Jachmich [d], A. Kukushkin [f], A. Loarte [g], G.F. Matthews [h], R.A. Pitts [a], J. Rapp [d], D. Reiter [d], E. Tsitrone [i], Contributors EFDA-JET Work Programme [1]

[a] *Centre de Recherches en Physique des Plasmas, Association EURATOM-Confédération Suisse, Ecole Polytechnique Fédérale de Lausanne, CRPP-EPFL, PPB 211, CH-1015 Lausanne, Switzerland*

[b] *Max-Planck-Institut für Plasmaphysik, EURATOM-Association, D-85748 Garching, Germany*

[c] *Max-Planck-Institut für Plasmaphysik, EURATOM-Association, D-17491 Greifswald, Germany*

[d] *FZJ-Forschungszentrum Jülich, Association Euratom-FZJ, D-52425 Jülich, Germany*

[e] *FOM-Inst. Plasmafysica, Association EURATOM/FOM, TEC, P.O. Box 1207, 3430 BE Nieuwegein, The Netherlands*

[f] *ITER International Team, Garching Joint Work Site, D-85748, Garching, Germany*

[g] *EFDA-CSU, Max-Planck-Institut für Plasmaphysik, D-85748, Garching, Germany*

[h] *UKAEA Fusion, Association Euratom-UKAEA, Culham Science Centre, OX14 3DB Abingdon, United Kingdom*

[i] *Association EURATOM-CEA, CEA Cadarache, 13018 St. Paul lez Durance, France*

Abstract

A campaign of pure helium discharges in the JET tokamak equipped with the MarkIIGB divertor has been performed. This paper describes some of the experimental observations of divertor detachment obtained in L-mode density ramp He discharges and presents a selection of results from the application of B2.5-Eirene code modelling to a JET He plasma. Detachment is very different from that observed in equivalent D discharges. Particle fluxes remain attached up to higher densities and, with decreasing input power, particle detachment occurs earlier in density. However, in contrast to comparable D plasmas, the low measured target T_e at all but the lowest n_e in helium leads to an earlier decrease in power flux. Simulations show that detachment is caused by the escape of He neutrals from the target vicinity where, together with the He^+ ions they radiate along the separatrix and above the X-point area, starving regions downstream of power.

PACS: 52.24.Vy; 52.25.Ya; 52.40.Hf; 52.55.Fa; 52.65.−y
Keywords: B2.5-Eirene; Detachment; Helium; Divertor; Tokamak; JET

1. Introduction

A number of intimately linked key factors determine the onset and nature of tokamak divertor detachment, some related to magnetic and divertor geometry (parallel field connection lengths, degree of neutral baffling, etc.) and many to details of distributed power loss in the divertor volume (momentum losses due to charge exchange and impurity and main plasma species line radiation). These volumetric losses are in turn governed by the material of first wall surfaces and the choice of fuelling gas. By exchanging deuterium for helium in a machine containing significant quantities of graphite, whilst retaining the important geometrical parameters, the effect on the character of detachment of a significant change in both the principal atomic physics processes

* Corresponding author. Tel.: +41-21 6936544; fax: +41-21 6935176.
E-mail address: macro.wischmeier@epfl.ch (M. Wischmeier).

[1] See annex of J. Pamela et al., Overview of recent JET results and Future Perspectives, FusionEnergy 2000 (Proc. 18th Int. Conf. Sorrento, 2000), IAEA Vienna, 2001.

0022-3115/03/$ - see front matter
PII: S0022-3115(02)01427-7

and the nature of the carbon impurity source can be studied. Helium plasma discharges with He neutral beam injection (NBI) and operating conditions matched to previous D discharges have been performed during a recent JET campaign in the MarkIIGB divertor configuration [1]. This paper concentrates on some of the key experimental observations of divertor detachment obtained in He L-mode density ramp discharges and presents a selection of results from B2.5-Eirene code modelling of these pulses.

2. Experiment

The discharges discussed here have $I_p = 2.5$ MA, $B_t = 2.4$ T, with strike points on the vertical divertor targets and are each characterized by a density ramp to the density limit with varying levels of He NBI power up to 5 MW. The mean purity level of the He plasma discharges is around 90%, measured both by visible spectroscopy in the plasma edge and by monitoring partial pressures in the subdivertor volume. As shown in Fig. 1, these pulses have low wall clearance in the main chamber (similar density limit pulses in high wall clearance configurations are described in a separate contribution to these proceedings [2]).

Fig. 2 compiles the density dependence of key strike point experimental data from both target Langmuir probes and IR thermography for the inner (Fig. 2(a)–(c)) and outer (Fig. 2(d)–(f)) targets. With the exception of the peak IR power (for which no data is available in D), the data are from three He discharges with varying P_{NBI} and a single D pulse for reference matched most closely to the He discharge #54001, corresponding to the mid-range power in the heating scan. Note the considerably higher density limit in He compared with D [2]. Fig. 2 shows clearly how the observed detachment in He is very different from that in D. At the inner divertor, particle (Fig. 2(a)) and energy (Fig. 2(c)) detachment occurs immediately in D. This is a common observation in JET discharges with the $B \times \nabla B$ drift direction towards the X-point [3].

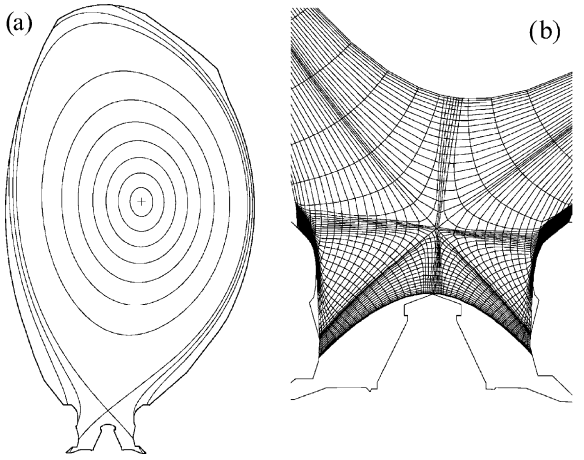

Fig. 1. (a) JET low clearance equilibrium referred to in this paper and the simulation grid (b) in the divertor region.

In equivalent He plasmas, inner target ion fluxes begin to decrease at much higher densities, with the onset of detachment coincident with the formation of a strong X-point MARFE. This MARFE occurs earlier in density as input power is decreased. In common with D plasmas, T_e at the inner target in He appears to be collapsed at all densities for the limited power scan described here (Fig. 2(c)). Note also the low peak powers (Fig. 2(b)), only just above the experimental sensitivity of the IR camera – although particles still arrive at the target, the energy flux is low, even at the maximum P_{NBI} of 5 MW.

At the outer target, particle flux detachment in He occurs at marginally higher $\bar{n}_e$ (Fig. 2(d)) in comparison with the inner target and is again sensitive to the degree of input power. In D for the reference case in Fig. 2, the outer target remains attached almost until the density limit, where the formation of an X-point and then rapidly an inner wall MARFE occurs [2]. The outer target electron temperatures (Fig. 2(f)) demonstrate clearly the effect of increasing input power, decreasing in He, as in D, to values of $\sim$5 eV as $\bar{n}_e$ increases. Unlike in D however, when T_e falls in the He plasma, the particle flux does not (as also observed in the inner divertor). In D, strong momentum loss is followed by recombination which ultimately decreases the particle flux [4]. Note that the known problems of Langmuir probe interpretation at low T_e prevent any knowledge of the true value of T_e at high $\bar{n}_e$ [5]. In He, for densities below the detachment threshold, the peak IR power at the outer target (Fig. 2(e)) falls in synchrony with T_e, despite the increasing ion flux (Fig. 2(d)).

Fig. 3 illustrates the behaviour for a single discharge of the total radiation (from bolometry) in the divertor region as $\bar{n}_e$ rises. Initially located at both the inner and outer strike zones at low $\bar{n}_e$, the total radiation increasingly concentrates at the inner leg and then finally above the X-point during the MARFE phase. Likewise, the HeI emission (HeI, 706 nm, from tomographic reconstruction of tangential CCD camera images [6]) begins at the outer and switches to the inner leg at high $\bar{n}_e$. At high density in He, CIII emission in the divertor and main chamber is observed to decrease to extremely low levels. This is unlike the case in D, in which this emission remains constant or even increases with increasing $\bar{n}_e$ [1,2]. This is attributed to the absence of chemical sputtering in He (and the decrease of ion energy below the threshold for physical sputtering at high $\bar{n}_e$) and implies that the radiated power (Fig. 3(b)) in He plasmas is due almost exclusively to that from He^0 and He^+ at elevated densities.

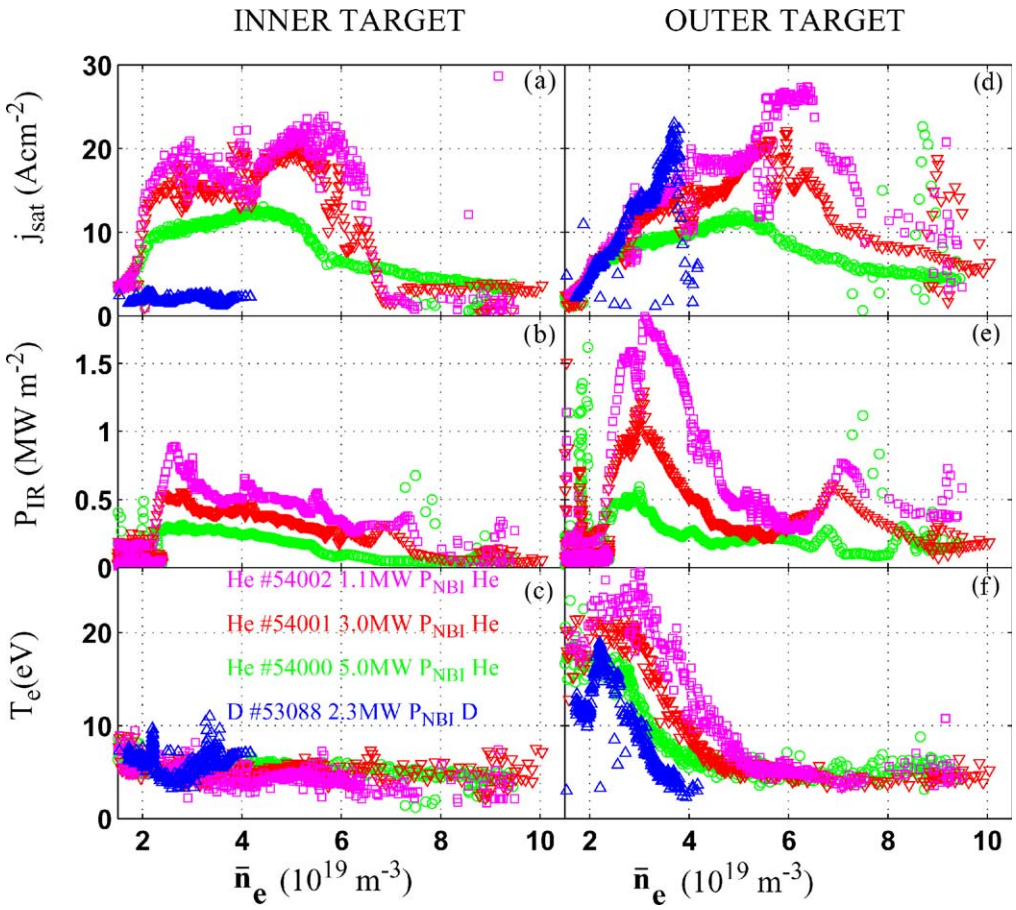

Fig. 2. Experimental measurments of the plasma density dependence of ion particle flux (a, d), peak surface heat flux (b, e) and electron temperature (c, f) at the inner (left) and outer (right) divertor targets. Data are shown for three He discharges and a single comparable D pulse, with the exception of P_{IR}, for which no measurements are available, in D.

3. Simulations

The SOLPS5 (B2.5-Eirene) code has recently been fully installed at JET and is now being routinely used for the simulation of D plasmas [7]. However, modelling the complex high-density detached cases has only just begun and the results are insufficiently mature to be included here. In helium, the absence of hydrocarbon chemistry and molecular species renders the situation somewhat less complex. The basic findings reported in this paper have much in common with those found in an earlier attempt at He plasma modelling [8] for DIII–D discharges with the older, SOLPS4 version of the code. The latter has also been used to simulate a single reference JET He plasma case and the results found to be in good agreement with those of SOLPS5 reported below.

The simulations are conducted on a grid (Fig. 1(b)) extending from $\rho = -4$ to 3 cm relative to the outer midplane separatrix – chosen so as to be compatible with concurrent EDGE2D-NIMBUS and UEDGE [9] modelling of similar discharges. Radial transport coefficients $D_\perp = 0.2$ m^2 s^{-1}, $\chi_\perp = 1.0$ m^2 s^{-1} are used in these first simulations – sensitivity studies to variations in these coefficients are underway.

Ion sputtering occurs only at the divertor targets in SOLPS5, whilst neutral interaction with divertor and main chamber walls is included in the model. Physical sputtering is implemented according to the Roth–Bodansky formula [10] with chemical sputtering (for the D minority) fixed at 1%. Concerning the percentage of D in these code runs, sensitivity tests have been performed for constant n_e and input power, P_{SOL} at the inner boundary of the simulation grid by varying the ratio of density due to D^+ and He^{2+} ions corresponding to D concentrations up to 40%. No significant change in the target profiles was observed throughout this concentration scan, in contrast to the findings for SOLPS5 simulations with horizontal target geometry [7]. This apparent sensitivity

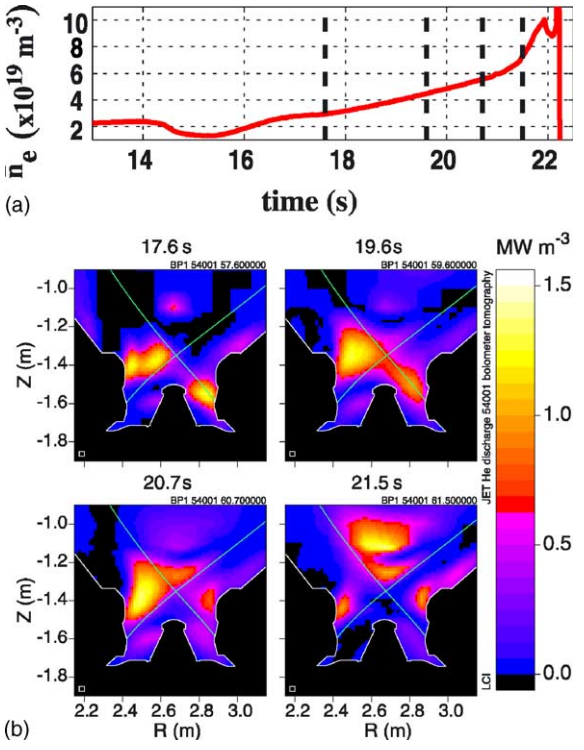

Fig. 3. Density dependence of the 2-D distribution of total radiation in the divertor for He discharge #54001. The bolometric inversions (b) correspond, in the clockwise direction starting from top left, to the times marked by the vertical dashed lines in the density trace (a). Note the intense emission from the inner divertor and the movement of radiation above the X-point at the highest density.

in the code to divertor geometry is the subject of ongoing study. For the results presented here, the D concentration was fixed at values below 8%.

For fixed $P_{SOL} = 3.8$ MW, comparable to discharge #54001 of Fig. 2, Fig. 4 compiles code output and target probe measurements, the latter averaged over 0.6 s intervals, at four different times in the density ramp for n_e, T_e and ion particle flux profiles across the outer and inner targets mapped to the outer midplane. Code output is plotted for four upstream separatrix densities in an attempt to simulate the experimental density ramp. The probe data are color coded, with each color referring to a time slice in the density ramp, corresponding to the four times highlightened by the vertical lines in Fig. 3(a). Agreement is in general reasonable given that transport coefficients have been fixed for code optimization and code comparison rather than providing the best match to upstream profiles. There is however a persistent tendency in the code to underestimate T_e in the strike point and private flux regions at all but the lowest densities.

This does not appear to be the case for comparable UEDGE and EDGE2D simulations in which T_e is well matched at the outer target, though none of the codes (drifts are not included) can match the inner/outer target asymmetries seen in experiment. Further SOLPS5 simulations are planned (variation of transport coefficients, P_{SOL}, etc.) in order to further investigate this interesting discrepancy.

In Fig. 5 the variation with n_e^{ib} (inner boundary density) of total ion and power flux to the targets shows that the general experimental observation (Fig. 2) in helium plasmas of power flux detachment occurring before particle loss is reproduced by the code. The simulations also demonstrate a clear tendency for lower total power flux to the inner target compared with the outer.

In the context of this study, the principle differences between He and D are the increased mean-free-path for neutral ionisation ($\lambda_{mfp}^{He} \sim 6\lambda_{mfp}^{D}$ at 10 eV) and the reduced CX reaction rates (factor of 3–4 at 10 eV). What happens is simply that neutral He recycled at the targets penetrates further upstream before being ionized than would be the case for D neutrals. Fig. 6 illustrates this effect from the point of view of the code. With increasing $\bar{n}_e$, the ionisation fronts for He^0 and He^+ move progressively further away from the targets to produce a strong radiating zone dominated by HeII line radiation, starving the divertor of power until pressure collapse prevents further ionisation and the target flux falls.

The main carbon sputtering mechanisms in these simulations are physical sputtering due to He^+ and He^{2+} ion impact, although D and D^+ contribute to the total sputtered flux at levels up to 30% due to the observed (in the simulations) accumulation of D^+ ions in the divertor region. At high densities, this contribution can amount to 25% of the total electron density in the target region. With increasing n_e^{ib}, the total carbon content in the simulations decreases by a factor of ~2 (the C ion fluxes always remaining negligible compared to the He ion fluxes at the targets), and the radiative losses due to CIII and CIV, reaching their maximum only at the lowest simulated densities, are always low (2–25%) compared to the losses from HeII.

4. Discussion and conclusions

In helium, divertor detachment begins at much higher upstream densities than in deuterium and is similar to that in D at most in the sense that the inner target detaches first. For varying input power, only at the highest densities and at high input power is particle detachment observed at both targets. Particle detachment occurs close to the density limit whilst power detachment is observed to occur at much lower densities. From comparison of simulations and experimental data

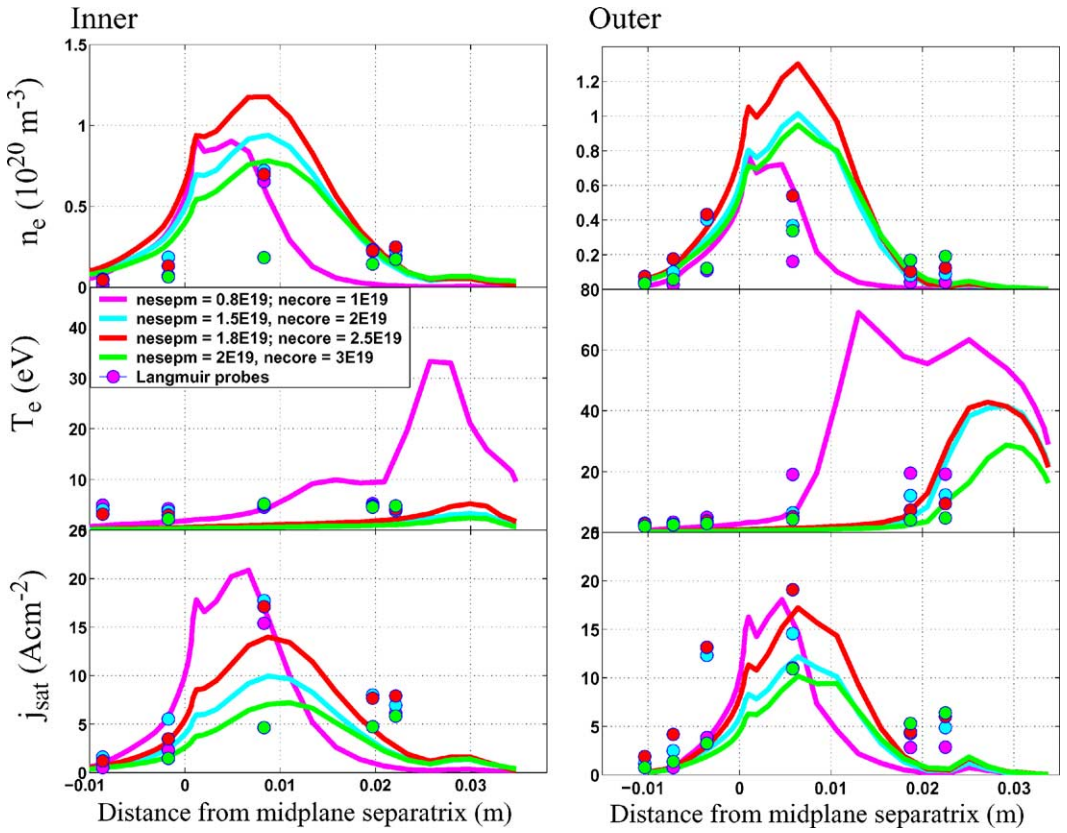

Fig. 4. Comparison of simulated (lines) n_e, T_e and j_{sat} with data from Langmuir probes (circles) at four values of $\bar{n}_e$ in pulse #54001 ($P_{NBI} = 3.0$ MW). Data are mapped to the outer midplane. 'necore' denotes the density at the inner boundary of the grid chosen for the simulations while 'nesepm' specifies the electron density at the separatrix at the outer midplane resulting from the simulations. The sequence of colors ●, ●, ●, ● refers to rising density and corresponds to the four times depicted in Fig. 3 in the case of the experimental data points. The experimental points are time averaged over 0.6 s. Note that the correspondence between code and experiment for nesepm is only approximate.

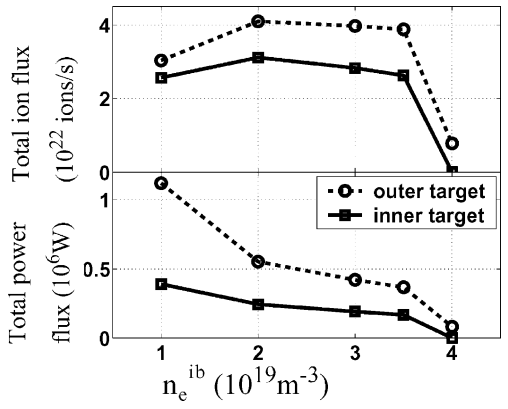

Fig. 5. Simulated total ion and power flux to the inner and outer targets indicating the experimental observation that power flux detachment occurs before particle flux detachment in He plasmas.

it is clear that the power detachment is a consequence of He atoms escaping further upstream compared to the case for D neutrals, followed by power loss, mostly due to He^+ line radiation. At the highest densities a large enough fraction of the power entering the SOL is lost through line emission that there is insufficient energy for ionisation of the recycled neutrals, thereby leading to a collapse in particle flux to the targets. This is very different to the situation in D plasmas where a complex interdependence between CX reactions, radiative cooling due to high carbon concentrations, recombination and ionisation processes lead to the observed power and particle detachments. In He, recombination processes play no role during detachment since insufficient momentum is removed by ion-neutral friction to allow residence times for He^+ in the divertor region to be sufficiently high for recombination to be effective as a sink of charged particles. Due to the few simple atomic key processes involved in the detachment of He plasmas

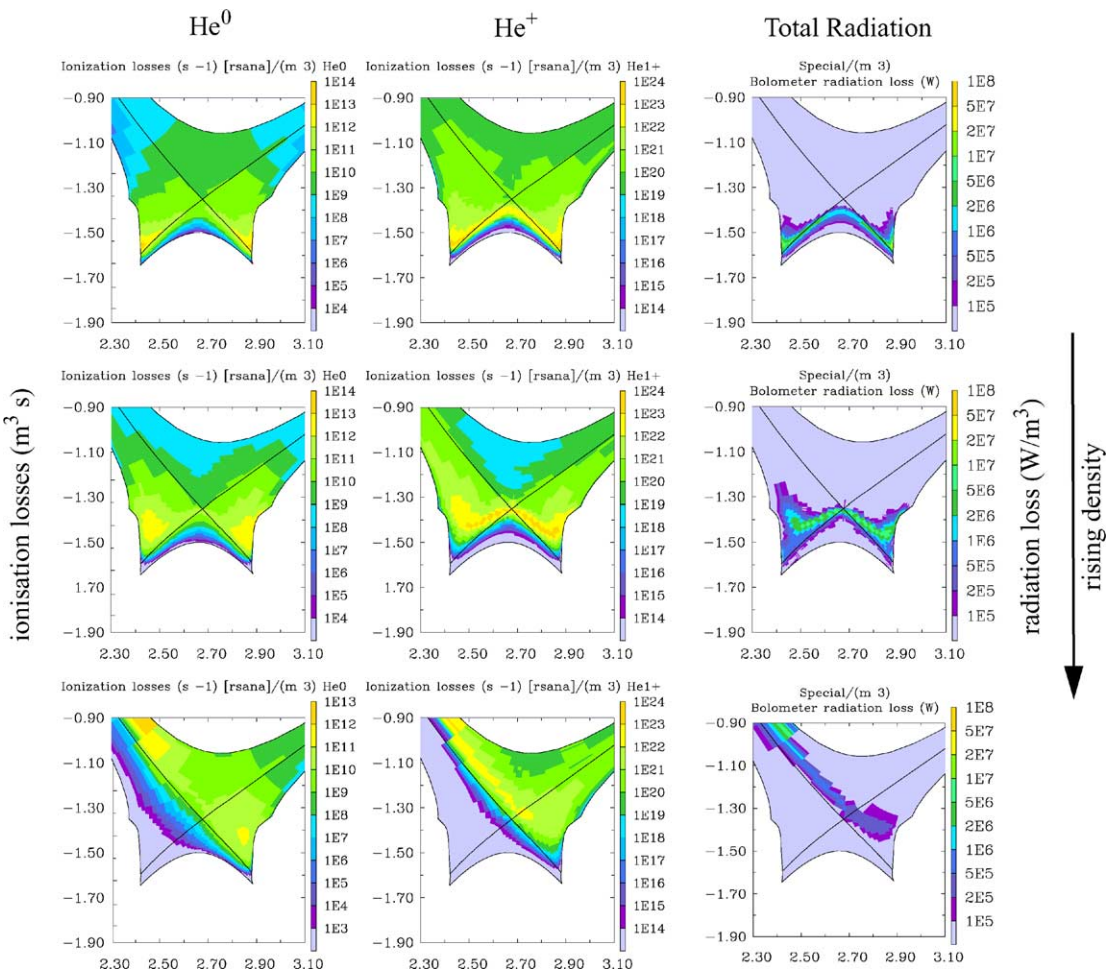

Fig. 6. Simulated ionisation loss rates for He^0 ($\times 10^{10}$) and He^+ and total radiation with increasing density based on conditions comparable with discharge #54001 at $P_{NBI} = 3.0$ MW.

(and the absence of molecular species) they are an ideal subject for benchmarking SOL codes. It is not yet clear why, for example, with vertical targets in the MarkIIGB divertor, B2.5-Eirene produces very low electron temperatures in the strike point and private flux regions compared to higher values simulated by UEDGE and EDGE2D-NIMBUS and measured by target Langmuir probes. Comparisons with SOLPS5 simulations for matched JET deuterium discharges are underway.

Acknowledgements

This work was performed under the European Fusion Development Agreement and was supported in part by the Swiss National Science Foundation, EURATOM and the UK Department of Trade and Industry.

References

[1] R.A. Pitts et al., these Proceedings, PSI-15. PII: S0022-3115(02)01429-0.
[2] J. Rapp et al., these Proceedings, PSI-15. PII: S0022-3115(02)01455-1.
[3] G. McCracken et al., J. Nucl. Mater. 266–269 (1999) 37.
[4] P.C. Stangeby, The Plasma Boundary of Magnetic Fusion Devices, IOP, 2000, ISBN 0 7503 0559 2.
[5] J. Horacek et al., these Proceedings. PII: S0022-3115-(02)01479-4.
[6] A. Huber et al., these Proceedings, PSI-15. PII: S0022-3115(02)01478-2.
[7] D. Coster et al., these Proceedings. PII: S0022-3115(02)01466-6.
[8] A. Loarte, Contrib. Plasma Phys. 40 (3&4) (2000).
[9] M. Fenstermacher et al., these Proceedings, PSI-15. PII: S0022-3115(02)01532-5.
[10] J. Roth, C. Gracia-Rosales, Nucl. Fusion 36 (1996) 1647.